AGU PUBLICATIONS

JGR

Journal of Geophysical Research: Space Physics

RESEARCH ARTICLE
10.1002/2016JA023774

Key Points:
- Ground-satellite conjugate observations of auroral finger-like structures
- Antiphase fluctuations of magnetic and plasma thermal pressure
- Pressure-driven instability in the magnetospheric source region

Supporting Information:
- Movie S1
- Movie S2

Correspondence to:
K. Nishi,
k-nishi@isee.nagoya-u.ac.jp

Citation:
Nishi, K., K. Shiokawa, and D. Frühauff (2017), Conjugate observation of auroral finger-like structures by ground-based all-sky cameras and THEMIS satellites, *J. Geophys. Res. Space Physics*, *122*, 7291–7306, doi:10.1002/2016JA023774.

Received 20 DEC 2016
Accepted 26 JUN 2017
Accepted article online 5 JUL 2017
Published online 15 JUL 2017

Conjugate observation of auroral finger-like structures by ground-based all-sky cameras and THEMIS satellites

Katsuki Nishi[1], **Kazuo Shiokawa**[1], **and Dennis Frühauff**[2]

[1]Institute for Space-Earth Environmental Research, Nagoya University, Nagoya, Japan, [2]Institute of Geophysics and extraterrestrial Physics, Technical University of Braunschweig, Braunschweig, Germany

Abstract In this study, we analyze the first conjugate observation of auroral finger-like structures using ground-based all-sky cameras and the Time History of Events and Macroscale Interactions during Substorms (THEMIS) satellites and investigated associated physical processes that are a cause of auroral fragmentation into patches. Two events are reported: one is a conjugate event, and the other is a nearly conjugate event. The conjugate event was observed at Narsarsuaq (magnetic latitude: 65.3°N), Greenland, at 0720–0820 UT (0506–0606 LT) on 17 February 2012. Analysis of the event revealed the following observational facts: (1) variation of parallel electron energy fluxes observed by THEMIS-E shows a correspondence to the auroral intensity variation, (2) plasma pressure and magnetic pressure fluctuate in antiphase with time scales of 5–20 min, and (3) perpendicular ion velocity is very small (less than 50 km/s). In the latter event, observed at Gakona, Alaska, on 2 February 2008, the THEMIS-D satellite passed across higher latitudes of finger-like structures. The data from THEMIS-D also showed the antiphase fluctuation between plasma pressure and magnetic pressure and the small perpendicular ion velocity. From these observations, we suggest that the finger-like structures are caused by a pressure-driven instability in the balance of plasma and magnetic pressures in the magnetosphere.

1. Introduction

Auroral emissions are caused by electron precipitation from the magnetosphere along Earth's magnetic field and project the magnetospheric plasma dynamics onto the ionosphere. Auroras are classified broadly into two types: discrete and diffuse [*Davis*, 1978]. A discrete aurora is characterized by its longitudinally stretched curtain-like structure and is considered to be a manifestation of the shear motion of plasma in the magnetosphere [e.g., *Haerendel*, 2007]. The intense brightness of discrete auroras is caused by the precipitation of electrons that are accelerated by field-aligned potential differences [e.g., *Reiff et al.*, 1988]. In contrast, a diffuse aurora has a glimmering brightness and does not have a specific shape, which distinguishes it from the discrete aurora. Pulsating auroras, one subclass of diffuse aurora, often become patchy structures. A possible origin of these patchy pulsating auroras is cold plasma irregularities in the magnetosphere [e.g., *Nakamura and Oguti*, 1987]. The electron precipitation in the diffuse auroral region is controlled by scattering of keV-energy electrons by electromagneric waves with frequencies of local electron cyclotron frequency. The wave generation is related to fluxes and temperature anisotropies of keV-energy electrons as well as density of ambient plasma [e.g., *Kennel and Petschek*, 1966].

Observations of these two major types of aurora have been made for a long time by using high-resolution all-sky imagers (ASIs) [e.g., *Mendillo et al.*, 1989; *Nishitani et al.*, 1994] or magnetospheric satellites [e.g., *Zhang et al.*, 2005; *Ebihara et al.*, 2010]. In recent years, simultaneous observations on the ground and in the magnetosphere have been reported [e.g., *Sato et al.*, 2015; *Donovan et al.*, 2008] and the "Conjunction Event Finder," a useful tool for finding conjugate observation events, was developed by *Miyashita et al.* [2011].

Recently, *Shiokawa et al.* [2010] found small-scale auroral finger-like structures, which are observed when diffuse auroras fall apart into patchy structures. They suggested that a pressure-driven instability between plasma and magnetic pressures in the magnetosphere could be a cause of these finger-like structures. Additional analysis of large-scale finger-like structures using ASIs was reported by *Shiokawa et al.* [2014]. The results of that analysis provided further support for the proposition that pressure driven instabilities were a cause of auroral fragmentation into patches through the finger-like structures. As described by *Shiokawa et al.* [2014],

the pressure-driven instability can be either interchange or ballooning instabilities. The interchange instability has zero wave number along the magnetic field line, and the whole magnetic flux tube moves together. Ballooning instability has a finite wave number along the magnetic field line. Both instabilities develop in the region where a force balance holds between earthward magnetic tension force and tailward pressure gradient force in the MHD fluid approximation [e.g., *Gold*, 1959; *Voronkov et al.*, 1997; *Cheng*, 2004; *Xing and Wolf*, 2007; *Kozlovsky et al.*, 2007; *Miura*, 2009]. *Hashimoto et al.* [2015] reported, through statistical studies of small- and large-scale finger-like structures, that finger-like structures start to develop when the substorm recovery phase starts and that they tend to be observed at post-midnight local times.

In these previous studies, conjugate observations at the ground and in the source magnetosphere were not analyzed to investigate auroral fragmentation through the finger-like structures. The purpose of this study is to investigate the physical processes occurring in the magnetosphere in association with auroral finger-like structures, by using cases for which the footprints of Time History of Events and Macroscale Interactions during Substorms (THEMIS) satellites pass across the finger-like structures observed by ground-based ASIs.

2. Instruments

In this study, we used plasma, electric field, and magnetic field instruments on board the THEMIS-D and THEMIS-E satellites [*Angelopoulos*, 2008] to obtain data associated with auroral finger-like structures in the magnetosphere. The plasma instruments are the electrostatic analyzer (ESA) [*McFadden et al.*, 2008] and the solid state telescope (SST) [*Angelopoulos*, 2008; *Angelopoulos et al.*, 2008; *Larson*, 2009]. The ESA measures fluxes and pitch angle distributions of low-energy (5 eV to 25 keV) ions and electrons. The SST measures the same information for high-energy (25 keV to 1 MeV) particles. The electric field and plasma waves are measured by the electric field instruments (EFI) [*Bonnell et al.*, 2008], which consist of four spherical sensors mounted on 20 or 25 m booms. The fluxgate magnetometer (FGM) [*Auster et al.*, 2008] measures the DC magnetic field. The sampling rate of these data for our analysis is the spin rate of the satellite, about 1 per 3 s. We also used the ground-based all-sky imagers and magnetometers in Canada and Greenland that form part of the THEMIS Ground-Based Observatory (GBO) [*Mende et al.*, 2008; *Harris et al.*, 2008]. These cameras have a high time resolution (cadence: 3 s) and a 256 × 256 pixel image resolution. Assuming that auroral emissions occur at an altitude of 110 km, the radius of the field of view of the imagers is about 600 km.

3. Observations

To find conjugate observation events, we investigated THEMIS ASI images and THEMIS footprints obtained from the Conjunction Event Finder over the period between October 2007 and December 2014. First, we searched for finger-like structures in THEMIS ASI images during which the THEMIS satellite was in the North American longitudinal sector. We found 67 finger-like structure events. Then, a detailed investigation of THEMIS footprints in these events produced only one conjugate observation event for which the THEMIS footprint crossed the finger-like auroral structures, and six near-miss events for which the THEMIS footprints passed near the finger-like structures. The THEMIS satellites pass across ~70°N at their apogee, while auroral finger-like structures tend to appear at ~65°N. This difference of latitudes leads to this rather small number of conjugate events.

The best conjugate event was observed at Narsarsuaq (magnetic latitude (MLAT): 65.3°N), Greenland, at 0720–0820 UT (05:06–06:06 LT) on 17 February 2012. First, we will discuss this best event. Then, we will discuss one of the near-miss events, observed at Gakona (62.4°N, 214.8°E, MLAT: 63.1°N), Alaska, on 2 February 2008.

3.1. Observation of the Conjugate Event (Event 1)

Figure 1 shows *H* component of ground-level magnetic field variations observed at Narsarsuaq and other stations at nearby latitudes from 2200 LT to 0600 LT. The two red lines in Figure 1 indicate the time interval during which the finger-like structures appear at Narsarsuaq. The auroral substorm occurs at about 0640 UT around Fort Churchill (58.8°N, 265.8°E, MLAT: 68.1°N), Canada. The time interval of finger-like structures corresponds to the substorm recovery phase. The fact that the finger-like structures appear during the substorm recovery phase matches the result of the statistical study by *Hashimoto et al.* [2015].

Figure 2 shows the north-south keogram of the all-sky imager data obtained at Narsarsuaq on 17 February 2012. The aurora gradually expands southward from ~0540 UT to ~0630 UT. The substorm onset at 0640 UT

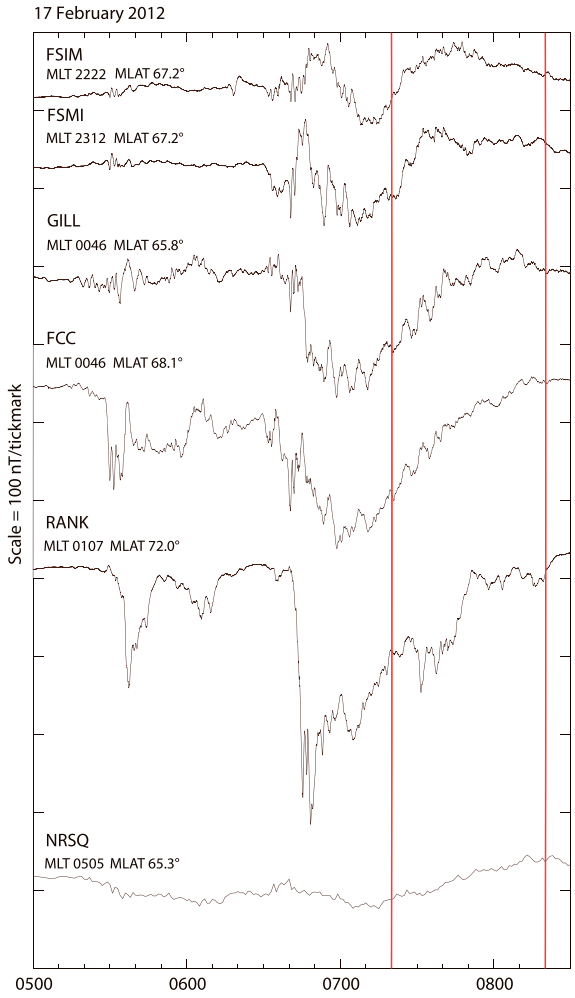

Figure 1. Ground-level *H* component magnetic field variations observed at Narsarsuaq and other stations at similar latitudes from 22 LT to 06 LT. The two red lines show the time interval during which the finger-like structures appear at Narsarsuaq.

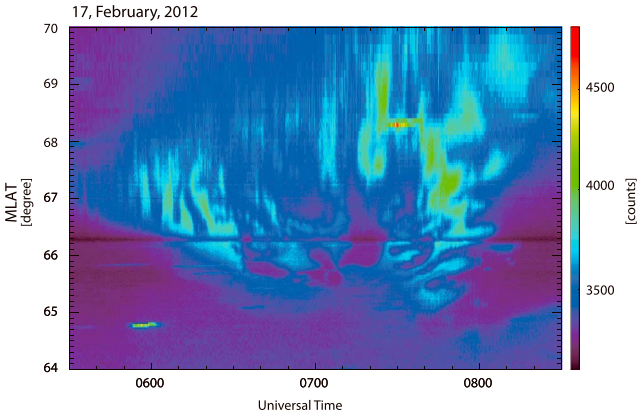

Figure 2. North-south keogram as a function of MLAT reproduced from all-sky images observed at Narsarsuaq for 05:00–08:30 UT on 17 February 2012. The boundary at 66.3°N is a part of line shadow in south part of the all-sky images.

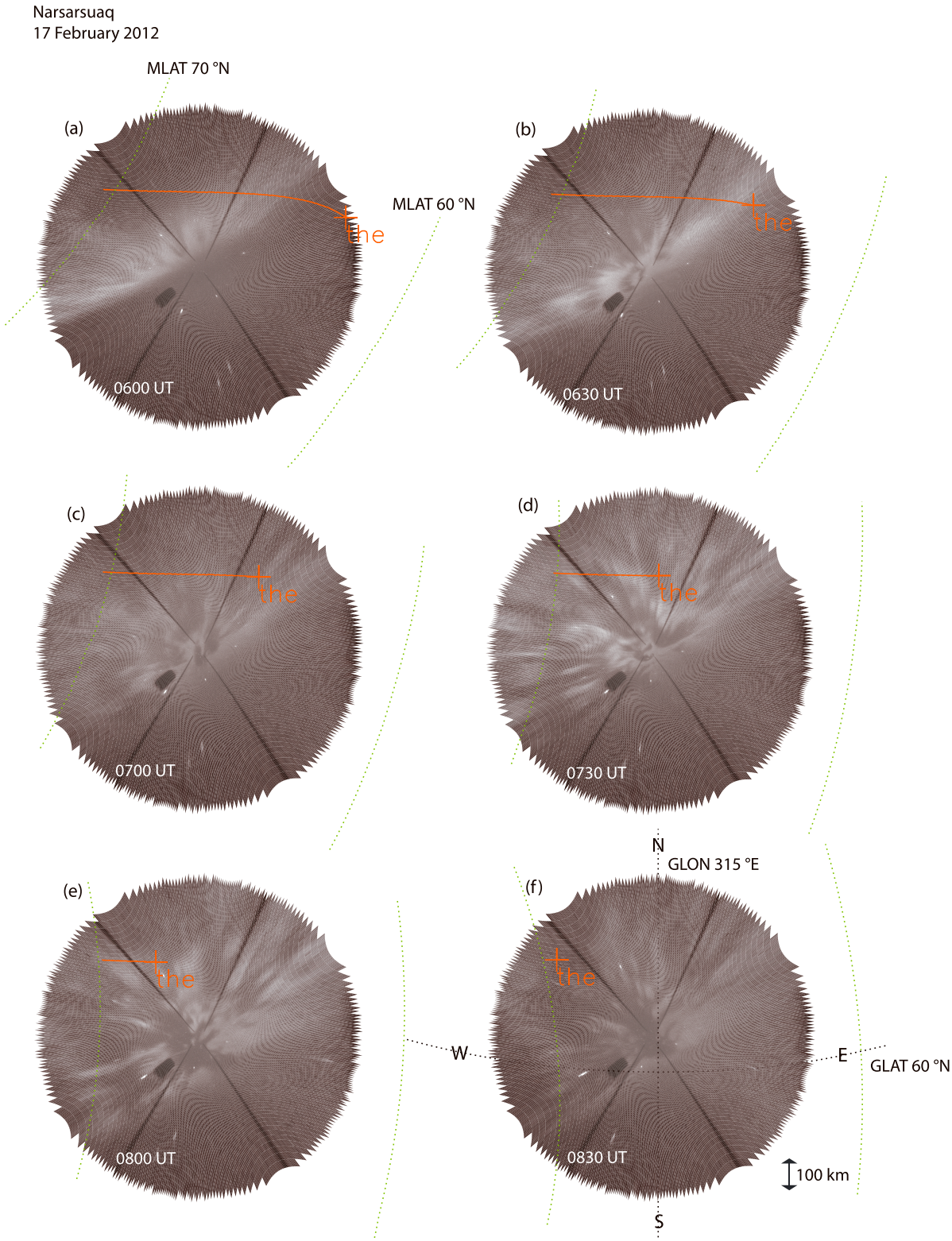

Figure 3. All-sky images taken at Narsarsuaq between 0600 UT and 0830 UT on 17 February 2012 with a 30 min interval. The orange lines in each image indicate the trajectory of the ionospheric footprint of the THEMIS-E satellite at an altitude of 110 km. The yellowish green lines indicate geomagnetic latitudes of 60°N and 70°N.

in the nightside local time sector seems not to affect these auroral features. We found auroral features corresponding to the finger-like structures which develop northward during 0600–0630 UT (0346–0516 LT) and during 0720–0800 UT (0506–0546 LT).

Figure 3 shows the auroral images taken by the all-sky camera at Narsarsuaq between 0600 UT and 0830 UT with a 30 min interval. The plus symbols indicate the footprint of the THEMIS-E satellite mapped onto the ionosphere, and the yellowish green lines indicate geomagnetic latitudes of 60°N and 70°N. The orange lines correspond to the trajectory of the footprint. This footprint is calculated using the Tsyganenko-96 magnetic field model [*Tsyganenko and Stern*, 1996]. Due to the discrepancy between the model and the real magnetic field, the footprint has some uncertainties, which we will discuss later. At 0600 UT, the finger-like structures start to develop northwestward. THEMIS-E comes into the auroral region at around 0630 UT and moves westward, passing across the finger-like structures several times from 0730 UT until 0830 UT in this figure.

Next, we will introduce the data obtained from the THEMIS-E satellite. Figure 4 shows the magnetic field and plasma differential energy fluxes observed by the THEMIS-E satellite during 0530–0830 UT. The satellite position is indicated below the bottom panel in GSM coordinates, where the satellite moves radially outward from 4.9 R_e to 8.8 R_e.

The solid curves in Figure 4a indicate the magnetic field variations. The blue, green, and red curves correspond to the GSM x, y, and z components of the magnetic field, respectively. The dashed lines are values obtained from the Tsyganenko-96 model. The difference between the two values is only about 10 nT, suggesting that it is reasonable to use this model for the field line mapping from the THEMIS satellite to the ionosphere (Figure 3). The magnitudes of the fields become smaller over time because the satellite was gradually moving away from the Earth.

The other four panels show the differential energy fluxes of electrons and ions. Figures 4b and 4c are ion fluxes obtained by the SST at energies of 25 keV to 6 MeV and the ESA at energies of 5 eV to 25 keV, respectively. Figures 4d and 4e show electron fluxes obtained by the SST at 25 keV to 1 MeV and the ESA at 5 eV to 25 keV, respectively. The high fluxes of both ions and electrons in Figures 4b and 4d before 0630 UT suggest that the satellite is in the radiation belt until 0630 UT. After 0630 UT, the ESA of THEMIS-E observed high electron fluxes at energies above 1 keV (Figure 4e). These fluxes probably correspond to the plasma sheet. In Figure 4e, we can see clear signatures of electron injection with an energy dispersion at energies above 1 keV at 0615–0650 UT. At 0650–0720 UT, two bands of electron fluxes at 10 keV and 1 keV are seen, suggesting that two injections occurred before the present event. The region at 0730–0830 UT when THEMIS-E crossed of finger-like structures corresponds to the plasma sheet electrons with energies of more than 1 keV and is outside (higher L shells) of these injection signatures in the magnetosphere.

Figure 5 shows a comparison of the satellite and ground auroral data for 0720–0830 UT. Figure 5a shows the auroral intensities in the footprint of THEMIS-E in the all-sky images shown in Figure 3. Figure 5b shows the electron energy flux parallel to the magnetic field by integrating the electron fluxes obtained by the ESA. In this panel, positive and negative values indicate northward and southward fluxes, respectively. Both the auroral intensities and the parallel electron fluxes show variations with time scales of 5–20 min. THEMIS-E is expected to be in the bright regions of the auroral finger-like structures at the local peaks in Figure 5a. The arrows between Figures 5a and 5b indicate a possible correspondence of peaks between the auroral intensity and the parallel electron flux. The correspondence between the peaks becomes worse for the third and fourth peaks, while the correspondence becomes better at fifth and sixth peaks. From this correspondence, we conclude that THEMIS-E passes across the bright regions of the finger-like structures at the peaks of parallel energy fluxes. The systematic time difference of a few minutes can be seen between the auroral intensity peaks and the electron flux peaks. Their maximum correlation coefficient is 0.51 with a time lag of ~120 s. We consider that this systematic time shift can be due to the ambiguity of field line mapping from the THEMIS-E satellite to the auroral ionosphere, rather than due to electron travel time from ~10 R_e to the ionosphere along geomagnetic field line, because the speed of 10 keV electron is ~9 R_e/s. As shown in Movie S1 in the supporting information, if the location of the satellite is slightly shifted southward or northward, the timing of the satellite crossing of bright finger-like structure can be easily shift for a few minutes. We have also tried to find better correlating footprints by shifting the footprint location to 5 or 10 pixels around the original footprints to the directions of north, east, south, and west. However, the correlation coefficient was not improved.

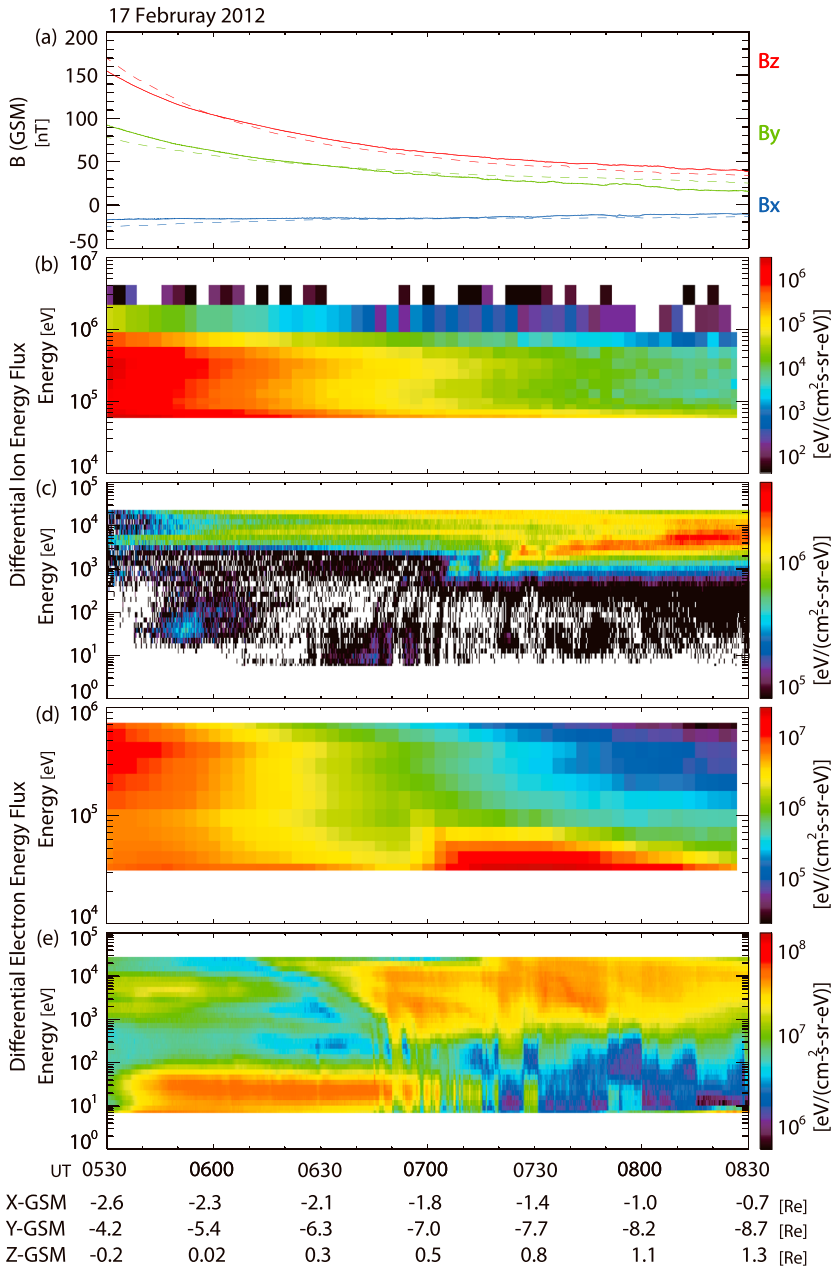

Figure 4. (a) The three-component magnetic fields in GSM coordinates observed by THEMIS-E (solid lines) and calculated by the Tsyganeko-96 model (dashed lines). The blue, green, and red curves indicate the *X*, *Y*, and *Z* components of the magnetic field, respectively. The lower panels show differential energy fluxes of (b) ions obtained by the SST, (c) ions obtained by the ESA, (d) electrons obtained by the SST, and (e) electrons obtained by the ESA. The numbers below the Figure 4 indicate the position of the THEMIS-E satellite.

Figure 5c shows the absolute value of the ion thermal pressure and magnetic pressure observed by the THEMIS-E satellite in red and black curves, respectively. The two pressures are comparable each other during the observation of the finger-like structures, indicating that this region is in the plasma sheet.

Figure 5d shows the deviation of the plasma pressure (red) and magnetic pressure (black) as measured by THEMIS-E. The plasma pressure contains both ion and electron pressures obtained by the ESA. Running 30 min averages were subtracted from the raw pressure data to show pressure variations shorter than 30 min clearly. We can see from this panel that the plasma and magnetic pressures fluctuate in antiphase with time scales of 5–20 min, indicating that these pressure variations are diamagnetic.

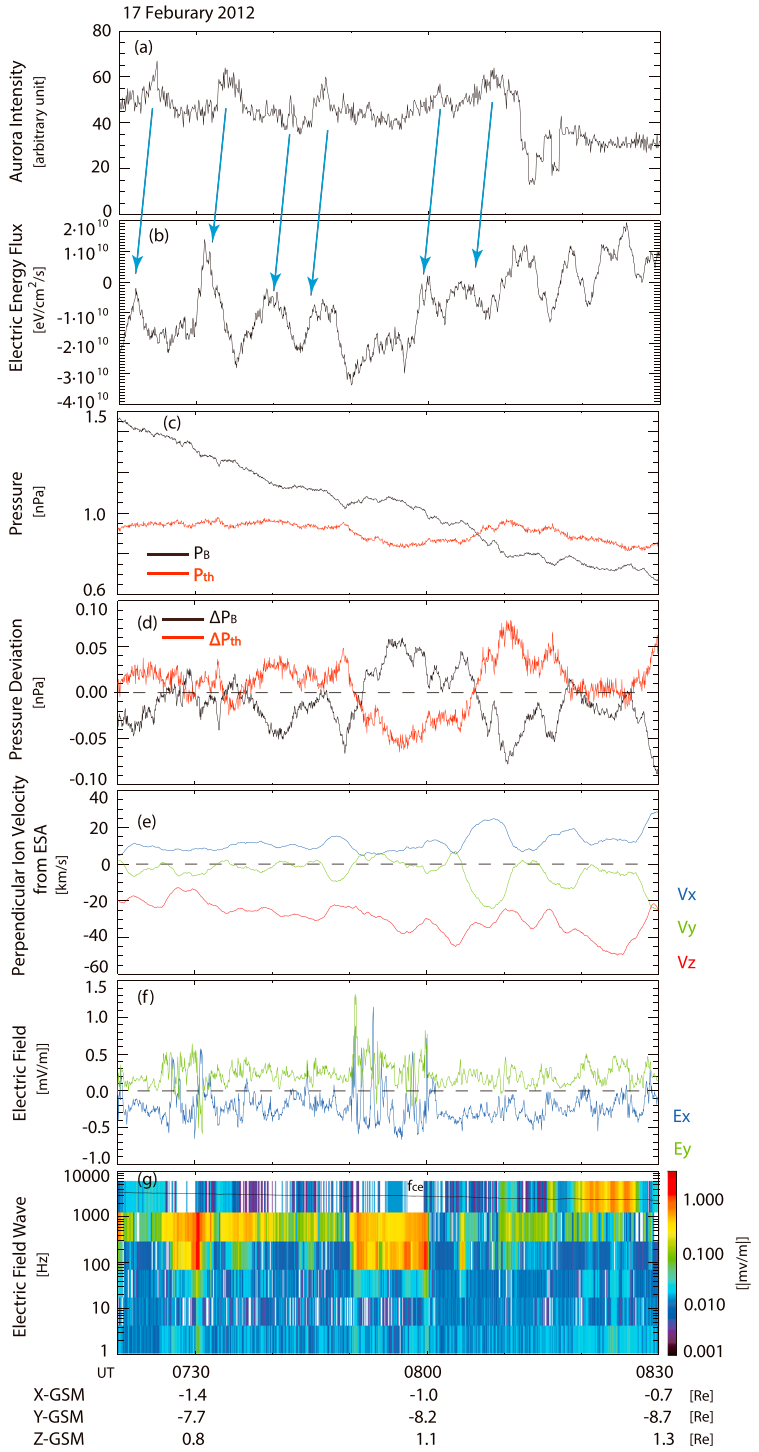

Figure 5. The top two panels show (a) auroral intensity at the satellite's footprint in the all-sky images and (b) electron energy fluxes parallel to the magnetic field obtained by the ESA. A positive value indicates fluxes which flow toward the Northern Hemisphere. The arrows between Figures 5a and 5b indicate a possible correspondence between the fluctuation peaks in the intensity and the flux. (c) The absolute value of thermal and magnetic pressure observed by THEMIS-E. (d) The thermal and magnetic pressure deviations observed by THEMIS-E. These values are obtained by subtracting 30 min running averages. (e) The ion velocity perpendicular to the magnetic field obtained from the ESA. The blue, green, and red curves show GSM *X*, *Y*, and *Z* components, respectively. (f) The electric field observed by the EFI. The blue and green lines indicate the GSM *X* and *Y* components, respectively. (g) The electric field wave spectra obtained from the EFI. The black line labeled f_{ce} indicates the electron cyclotron frequency. The numbers below the panels show the position of the THEMIS-E satellite.

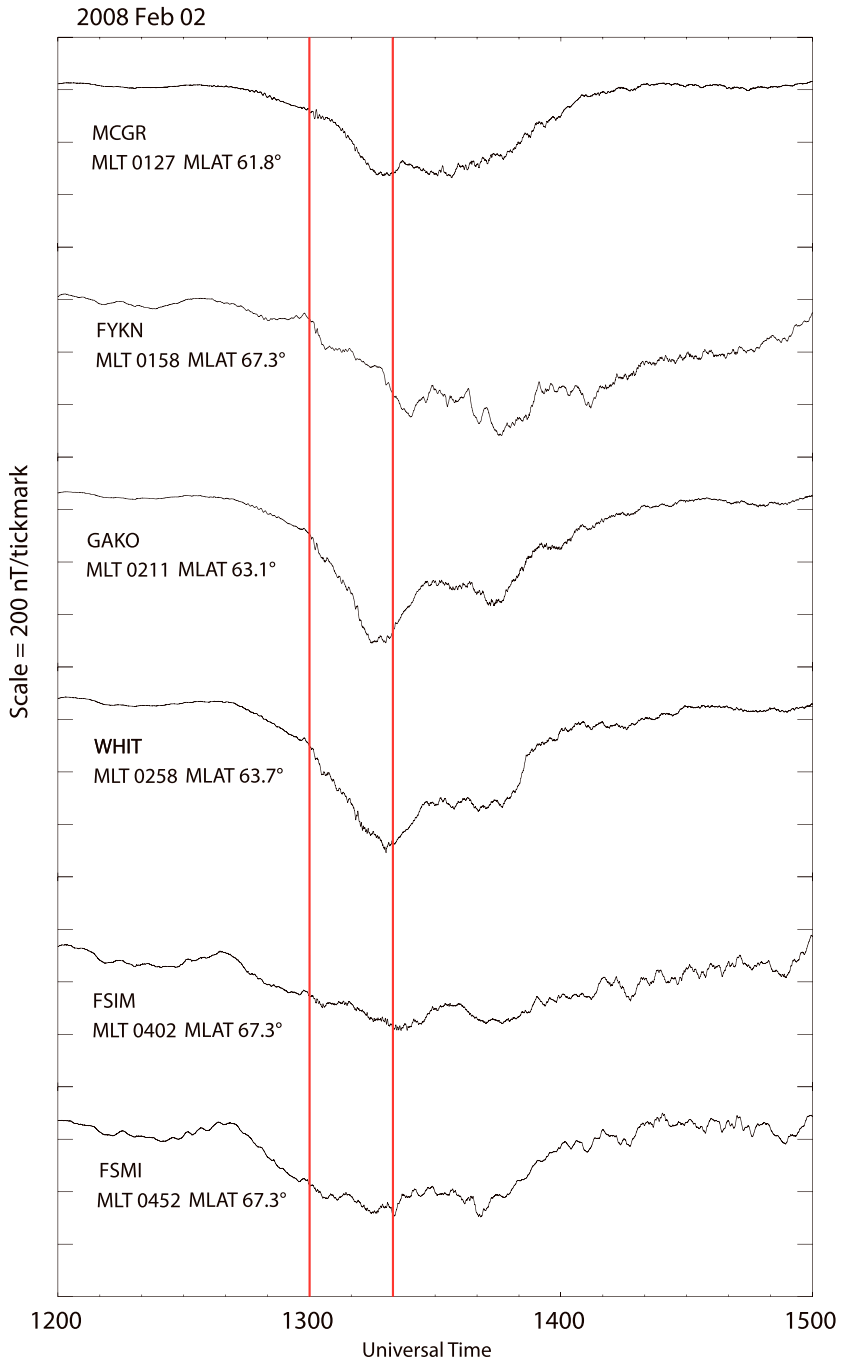

Figure 6. Ground-level *H* component magnetic field variations observed at Gakona and other stations at similar latitudes from 0130 LT to 0500 LT. The two red lines show the time interval during which the finger-like structures appear at Gakona.

Figure 5e shows three component ion velocities perpendicular to the magnetic field. These ion velocities are measured by the ESA. We find that perpendicular ion velocity is very low (less than 50 km/s) in the plotted interval, indicating that the finger-like structures are not related to high-speed earthward flows, such as bursty bulk flow (BBF) [*Angelopoulos et al.*, 1992].

Figure 5f shows the electric field variations observed by the EFI. The blue and green lines indicate the GSM *X* and *Y* components of the electric field, respectively. In the magnetic equatorial plane, the *X* component of the electric field corresponds to the radial direction of $E \times B$ drift of the plasma, while the *Y* component corresponds

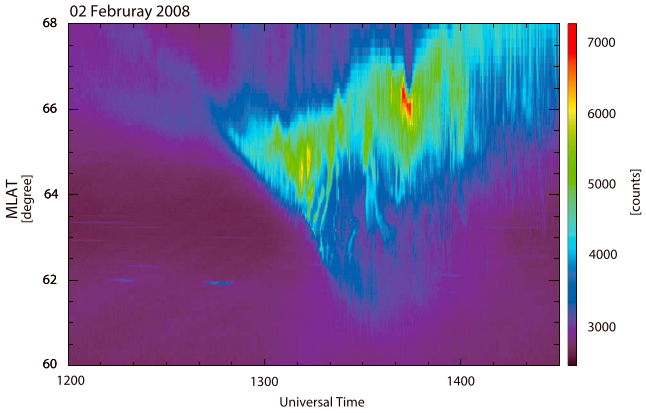

Figure 7. North-south keogram as a function of MLAT reproduced from all-sky images observed at Gakona for 05:00–08:30 UT on 2 February 2008.

to the azimuthal direction. We can see large fluctuation during 0750–0800 UT when the thermal pressure starts to decrease. The negative E_x and positive E_y corresponds to sunward and inward plasma motion, while the plasma flow data in Figure 5d show weak sunward ($V_x > 0$) and outward ($V_y < 0$) motion of plasma. The values of 0.2–0.5 mV/m correspond to the drift speeds of 5–13 km/s, which are comparable to the particle data in Figure 5d, and is very small compared with the speed of bursty bulk flow.

Figure 5g shows the wave spectra in the electric field data of EFI. At 0720–0830 UT, we can see the intensification of rather monochromatic waves at frequencies of 0.1–1 kHz, which probably correspond to the electron cyclotron harmonic (ECH) waves. The correlation between these ECH wave intensities and parallel electron fluxes is not clear. Similar ECH waves above diffuse/pulsating aurora have been reported by several previous papers [e.g., *Liang et al.*, 2010; *Nakajima et al.*, 2012].

3.2. Observation of the Near-Miss Event (Event 2)

This event is one of the six near-miss events. The all-sky camera in Gakona captured clear finger-like structures in the event. During the appearance of the finger-like structures, the THEMIS-D satellite passed across the sky of Fort Yukon, which is located north of Gakona. Unfortunately, cloud prevented the all-sky imager at Fort Yukon from capturing the aurora.

Figure 6 shows ground-level magnetic field variations observed at Gakona and other stations, in the same format as in Figure 1. The red lines indicate the time interval of finger-like structures observed at Gakona. According to Figure 6, an auroral substorm occurred around 1240 UT and the finger-like structures appeared during the expansion phase of this substorm.

Figure 7 shows the north-south keogram of all-sky images taken at Gakona for a time interval of 1200–1430 UT. The aurora started to develop southward at around 1250 UT, about 10 min after the start of substorm. The auroral finger-like structures appear at around 1300 UT, and their bright regions start to develop northward, although it is difficult to see the direction of their development in this keogram. Then, the finger-like structures became well-developed and auroral patches prevails in the auroral images around 1330 UT. Additionally, the north-south prolonged structure around 1335 UT corresponds to a torch-like structure that appeared after the appearance of the finger-like structures.

Figure 8 shows the images taken by all-sky imager at Gakona and Fort Yukon from 1300 UT to 1320 UT with a 5 min interval. As mentioned earlier, the sky at Fort Yukon was covered with cloud. The auroral finger-like structures develop northward between 1300 UT and 1315 UT. Then, the finger-like structures fragment into patches, as shown in Figure 8. The footprints of THEMIS-D were in the field of view of the camera at Fort Yukon, which is at latitude ~4° higher than the finger-like structures.

Figure 9 shows the background magnetic field and plasma energy flux data obtained by the THEMIS-D satellite. The format of this figure is the same as that of Figure 4. In Figure 9a, the magnetic field intensity of this event is smaller than that of Event 1 because the distance from the satellite to the Earth was larger in this case. The difference of magnetic field intensities between the observations and values modeled by Tsyganenko-96 is at most about 20 nT. Compared with Event 1, it seems that the fluctuation of the magnetic field is larger.

In Figures 9c and 9e, we can see high ion and electron energy fluxes at energies of several kiloelectronvolts between 1200 and 1310 UT, suggesting that the THEMIS-D satellite was located in the plasma sheet at this time interval. Both the ion and electron energy fluxes at energies above 10 keV start rising at 1310 UT. According to Movie S2, this increase of the fluxes suggests that the THEMIS-D satellite was at the magnetospheric counterpart of the extended auroral activity observed at Inuvik.

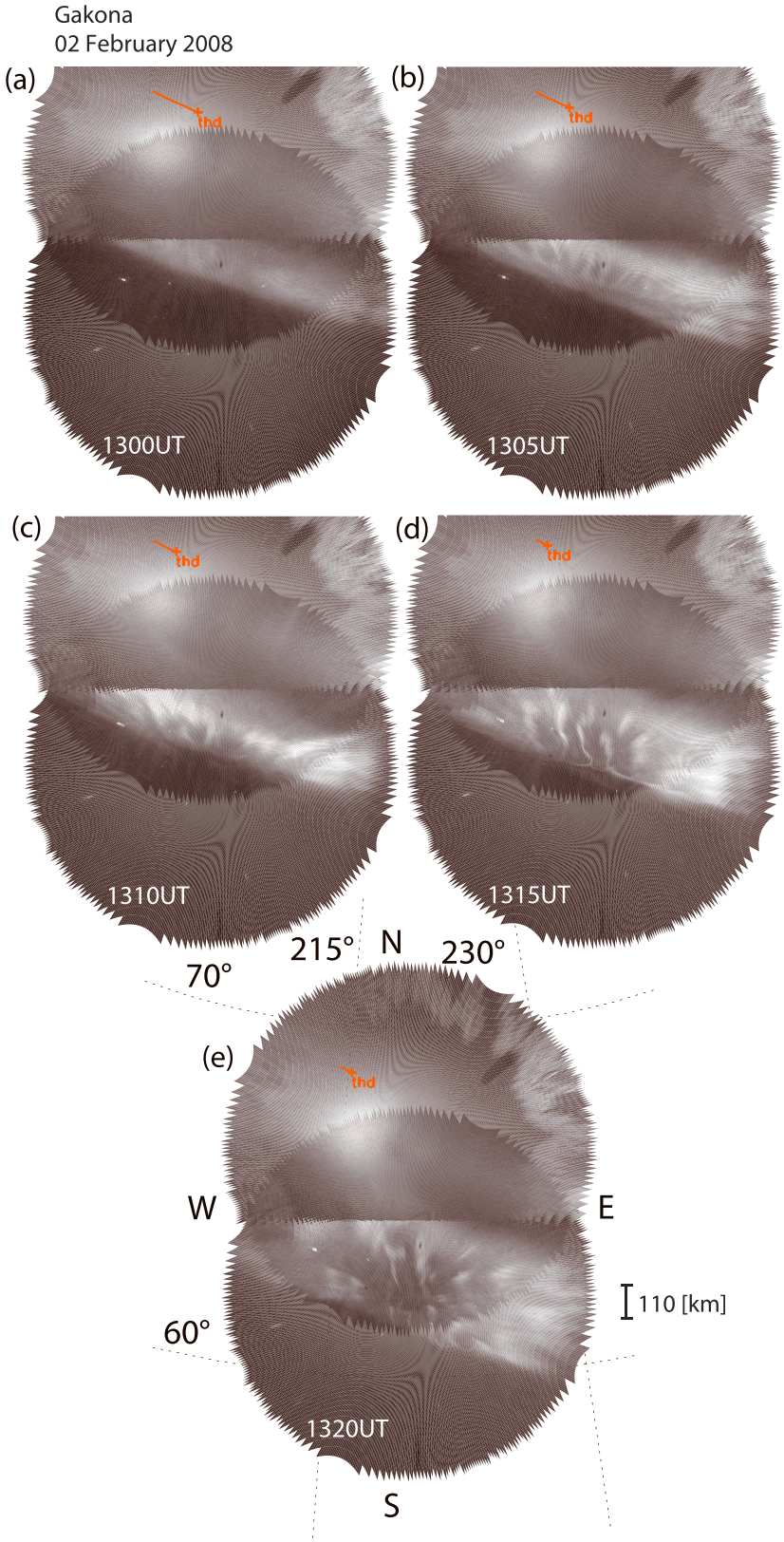

Figure 8. All-sky images taken at Gakona between 13:00 UT and 13:20 UT on 2 February 2008 with a 5 min interval. The orange lines in each image indicate the trajectory of the ionospheric footprint of the THEMIS-D satellite at an altitude of 110 km.

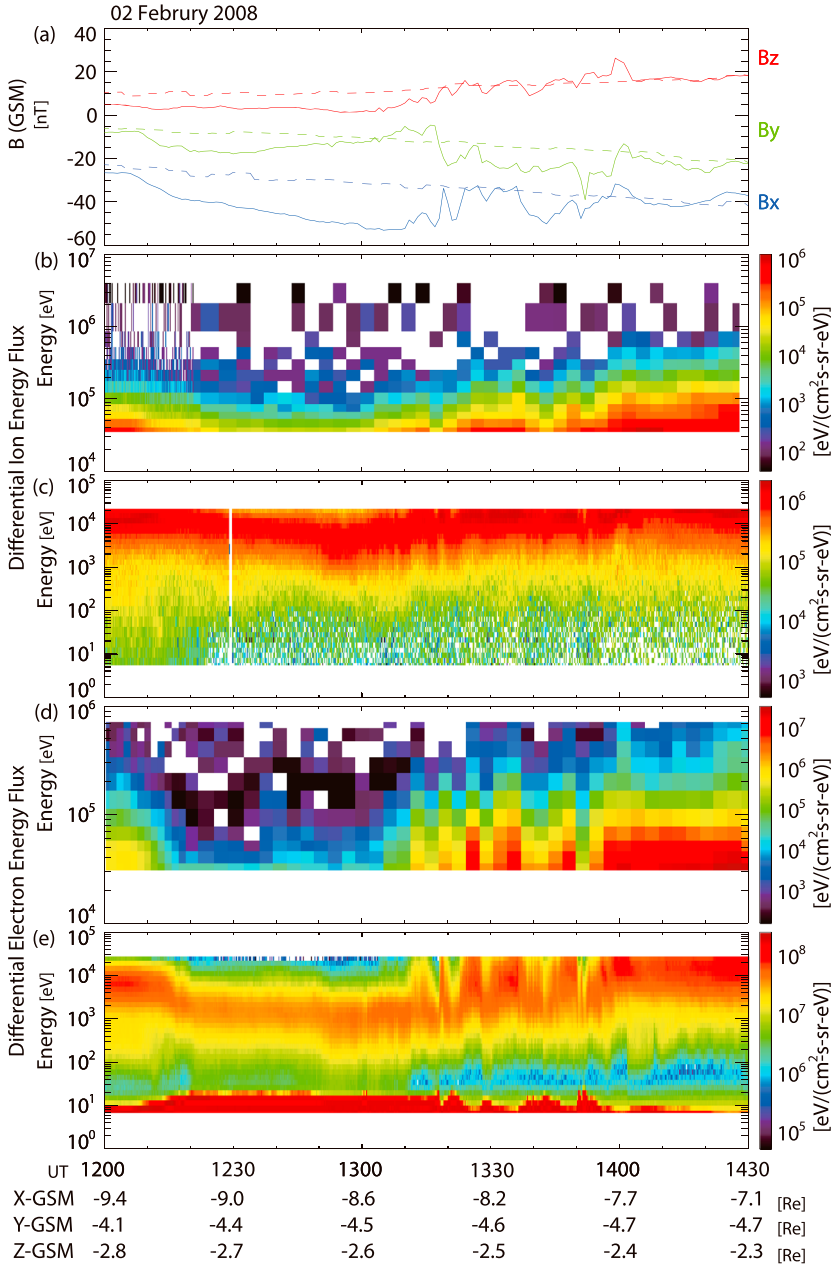

Figure 9. (a) The three-component magnetic fields in GSM coordinates observed by THEMIS-D (solid lines) and calculated by the Tsyganeko-96 model (dashed lines). The blue, green, and red curves indicate the *X*, *Y*, and *Z* components of the magnetic field, respectively. The lower panels show differential energy fluxes of (b) ions obtained by the SST, (c) ions obtained by the ESA, (d) electrons obtained by the SST, and (e) electrons obtained by the ESA. The numbers below Figure 9e indicate the position of the THEMIS-D satellite.

Figure 10 shows magnetic and plasma pressures and ion velocities obtained by THEMIS-D during this event. According to Figure 9, the dominant energy range of both the ion and electron fluxes is several kiloelectronvolts, so we use the data obtained by the ESA to estimate the plasma pressure in Figure 10. In Figure 10a, we can see antiphase fluctuations between the two pressures, which are similar to those in Figure 5c, for almost all the time period. However, antiphase fluctuation is not observed during 1300–1310 UT, when the finger-like structures started to appear at Gakona. This exception may be due to a sudden intensification of the magnetospheric magnetic field associated with substorm tail current disruption, breaking the balance between magnetic and plasma pressures.

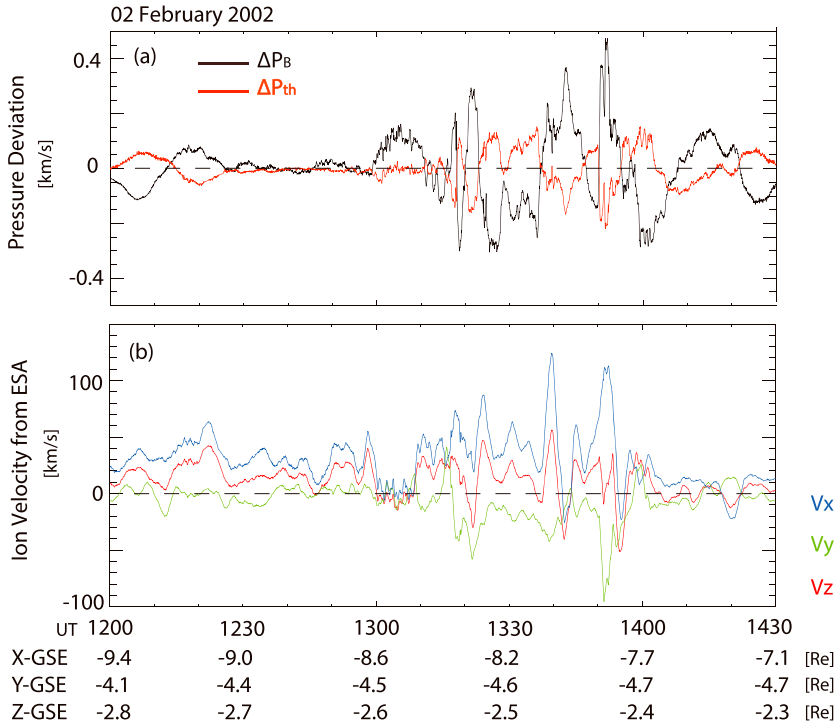

Figure 10. (a) The thermal and magnetic pressure deviations observed by THEMIS-D. These values are obtained by subtracting 30 min running averages. (b) The ion velocity perpendicular to the magnetic field obtained from the ESA. The blue, green, and red curves show GSM *X*, *Y*, and *Z* components, respectively. The numbers below the panels show the position of the THEMIS-D satellite.

Figure 10b shows the ion velocity perpendicular to the magnetic field as obtained by the ESA. The velocities are smaller than 100 km/s in almost all parts of the Figure 10b, suggesting that the BBF is not associated with the finger-like structures. We can see a sudden decrease of the perpendicular ion velocity during 1300–1310 UT, when the magnetic pressure increases at the substorm expansion phase.

4. Discussion

We have reported two finger-like structure events in this paper. One is a conjugate observation by a ground-based all-sky imager and a THEMIS satellite flying in the magnetosphere near the same field line of the finger-like structure (Event 1). The other is a near-miss event in which the THEMIS footprint passes at higher latitudes than those of the finger-like structures (Event 2). Event 1 was observed in Narsarsuaq, Greenland, on 17 February 2012, and Event 2 was observed in Gakona, Alaska, on 2 February 2008.

Figure 11 is a schematic illustration of the possible source region of the finger-like structures in the magnetosphere, based on the observation of Event 1 (top view from above the North Pole). A wavy line shows the finger-like structures which is considered to be the force balance surface between the magnetic pressure P_B and plasma pressure P_{th}. The shaded area shows the auroral bright region in which the plasma pressure is high, and the other area shows the auroral dark region in which the magnetic pressure is high. A curved red vector shows the trajectory of the THEMIS-E satellite moving from nightside to dayside in the dawn sector.

The antiphase fluctuation of the magnetic pressure and plasma pressure shown in Figure 5c implies that the THEMIS-E satellite passes across auroral bright and dark regions alternately, as shown in Figure 11. Given that these regions correspond to the source region of auroral finger-like structures, the antiphase fluctuation of the pressures supports the idea that pressure-driven instability is a cause of the development of finger-like structures. Additionally, we consider that the macroscale pressure-driven instability can cause corresponding variations of ambient plasma density that controls generation and propagation of kilohertz waves. Thus, the pressure-driven instability can create the observed auroral finger-like structures.

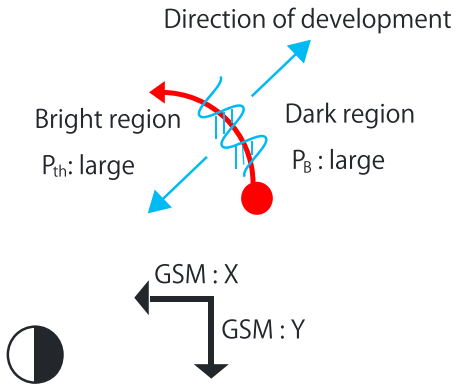

Figure 11. A schematic illustration of the possible source region of the finger-like structures in the magnetosphere (top view from the North Pole).

Similar diamagnetic (antiphase) pressure fluctuations have been reported for the drift mirror mode instability in the plasma sheet [e.g., *Vaivads et al.*, 2001; *Rae et al.*, 2007]. For the present event, we checked the criteria of drift mirror instability, which is expressed as follows [e.g., *Treumann and Baumjohann*, 1997]:

$$\sum_s \frac{\beta_{s\perp}^2}{\beta_{s\parallel}} > 1 + \sum_s \beta_{s\perp} \quad (1)$$

The result of this calculation for Event 1 is shown in Figure 12. This figure clearly indicates that Event 1 does not satisfy the drift mirror condition of equation (1). Thus, we conclude that the diamagnetic variations observed for the present event is not by the drift mirror instability.

The footprints of the THEMIS satellites in Figure 3 are calculated by the Tsyganeko-96 magnetic field model in this study. It is, therefore, necessary to estimate the ambiguity of this field line mapping. In order to estimate this ambiguity, we shifted the position of the satellite in the magnetosphere. When the position is shifted by $-0.5\ R_e$ ($1\ R_e = 6371$ km) in the direction of the GSM Y axis, the footprint shifts northward about 60 km from the original footprint at 0730 UT. Therefore, we can reasonably assume that 0.5 R_e in the magnetosphere (GSM Y direction) is mapped onto 60 km in the ionosphere (latitudinal direction). The difference between the original magnetic field value and the shifted magnetic field value is about 11 nT ($\Delta B_x = 0.6$ nT, $\Delta B_y = -7.7$ nT and $\Delta B_z = 8.3$ nT) in the Tsyganenko-96 magnetic field model. The difference between the modeled and observed magnetic field values is also about 10 nT ($\Delta B_x = -1.7$ nT, $\Delta B_y = -7.7$ nT, and $\Delta B_z = -6.6$ nT). Comparing these results, the uncertainty of the calculated footprint is estimated to be several tens of kilometers. Since the north-south scale of the finger-like structures is more than 100 km in Figure 3, we consider that the THEMIS-E satellite was in the magnetospheric source region of the finger-like structures.

As estimated from the Tsyganenko-96 model, the northward development of the aurora in the ionosphere is mapped onto the negative GSM Y direction in the magnetosphere at around 07:30 UT in Event 1. We measured the northward speed of development of the finger-like structure by comparing the two successive auroral images shown in Figure 13. Vectors in Figures 13a and 13b indicate the tip of an auroral finger-like structure, showing a slight extension to the north. The length of the northward development is about 35 km between these two images, giving a growth rate of about 145 m/s. Considering that 60 km northward in the ionosphere is mapped onto $-0.5\ R_e$ in the GSM Y direction in the magnetosphere, we obtain a development speed of −7.7 km/s in the direction of the GSM Y axis for the finger-like structure in the magnetosphere. Comparing to the GSM Y component of perpendicular ion velocity shown in Figure 5d (green line), the estimated development speed is comparable to the perpendicular ion velocity, though this small velocity may be within the ambiguity of THEMIS momentum measurements due to the upper boundary of the measurable energy (25 keV) of the ESA.

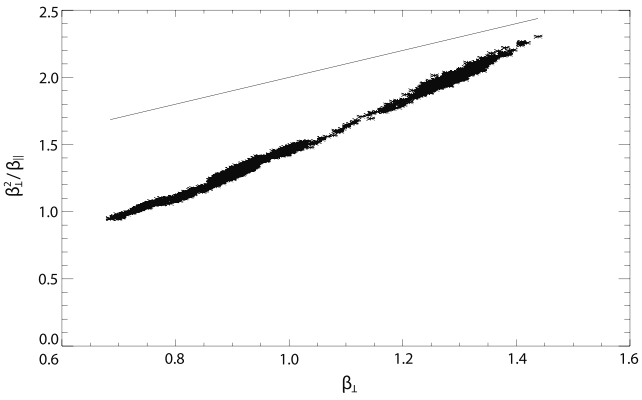

Figure 12. Mirror mode criteria check for the THEMIS-E satellite during Event 1. The solid line indicates $1 + \beta_\perp$.

Hashimoto et al. [2015] reported based on multiple event study (14 events) that finger-like aurora structures tend to develop when the substorm recovery phase starts and *AL* index starts to increase. In Event 1, the finger-like structures started to develop during the substorm recovery phase, as shown in Figure 1, though the Event 2 was observed during substorm expansion

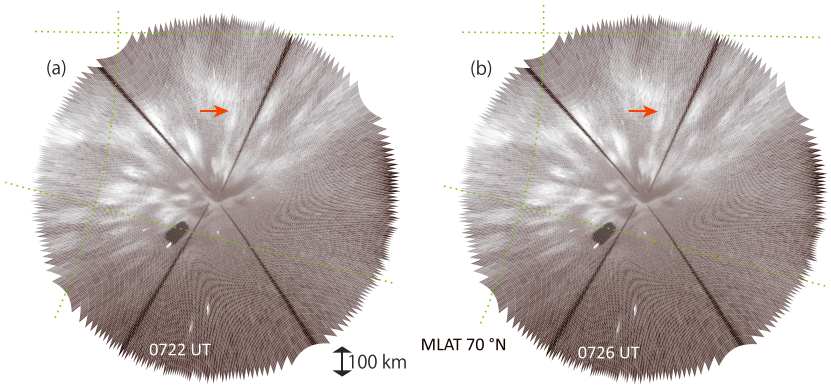

Figure 13. All-sky images showing the development of the finger-like structure. Orange arrows indicate the northern edge of the finger-like structure. The yellowish green lines indicate geomagnetic latitudes of 60°N and 70°N.

phase. The start of the finger-like structure at the start of the substorm recovery phase suggests that the ceasing of earthward flow at the recovery phase may be a trigger of the pressure driven instability.

In both cases, the finger-like structures appeared near the equatorward boundary of auroras. For our first case, the particle data obtained by the THEMIS-A satellite (not shown) indicate that THEMIS-A was in the plasma sheet at ~2 R_e inside of the THEMIS-E satellite in the same longitudinal sector. This indicates that the THEMIS-E was located at the equator boundary of the aurora and not at the inner boundary of the plasma sheet. The equatorward auroral boundary at magnetic latitudes of ~65° probably does not correspond to the inner boundary of the plasma sheet, because the typical inner boundary of the plasma sheet is well less than $L = 4$ (magnetic latitude of ~60° [e.g., *Ejiri. M. et al.*, 1980; *Kistler et al.*, 1992]). The equatorward auroral boundary can be an inner boundary of electron precipitation region where electrons have sufficient energy flux to produce observable auroral emission. The present observation suggests that the instability occur at least in the morning sector in the inner part of the plasma sheet at ~8 R_e.

In Figures 5b and 5c, the correspondence between the parallel electron fluxes and pressure variations is not so clear. We can discuss this possible correspondence using MHD equations of field-aligned currents. Assuming that the inertial current is small compared to the diamagnetic current, because the observed ion velocity in Figure 5d is very small, the current perpendicular to the magnetic field can be expressed as follows:

$$\mathbf{J}_\perp = \frac{\mathbf{B} \times \nabla P_{\mathrm{th}}}{B^2} \tag{2}$$

From the current continuity and omitting the plasma flow shear and inertial current, we can obtain the field-aligned current driven by the divergence of this perpendicular current as follows [*Hasegawa and Sato*, 1979]:

$$\mathbf{J}_\parallel = \mathbf{B} \int \frac{2}{B^2} \mathbf{J}_\perp \cdot \nabla B \mathrm{d}s_\parallel \tag{3}$$

We can recognize from these equations that $J_\parallel$ should correspond to the peak of ∇P_{th} rather than P_{th}. This can be a reason why we do not see good correspondence between P_{th} in Figure 5c and electron fluxes in Figure 5b, though the carrier of the possible upward field-aligned current in the auroral finger-like structure is still not clear. At least we can see variations of similar time scales (5–20 min) in both data. It is difficult to estimate ∇P_{th} from the single-satellite measurements.

5. Conclusion

In this study, we analyzed the first conjugate observation of auroral finger-like structures in ground-based all-sky imagers and magnetospheric THEMIS satellites. The observed plasma and magnetic field variations in the source magnetosphere are useful for understanding the physical mechanisms that may create the finger-like structures.

In the conjugate event, observed at Narsarsuaq (MLAT: 65.3°N), Greenland, the finger-like structures started to develop at 0720 UT during a substorm recovery phase. The THEMIS-E satellite passed across the finger-like

structures several times until 08:30 UT. The finger-like structures had spatial scale of 30–200 km and exhibited various directions of development. The electron energy fluxes parallel to the magnetic field at THEMIS-E and the auroral intensity in the footprint of THEMIS-E showed variations with time scales of 5–20 min and tend to have a one-to-one correspondence. This result implies that the THEMIS-E satellite passes across the bright regions of the finger-like structures at the peaks of the parallel electron flux. The deviation of the magnetic and plasma pressures showed antiphase fluctuations, again with the time scale of 5–20 min. This antiphase variation does not contradict to the idea that the pressure-driven instability in the plasma sheet caused the auroral finger-like structures. The ion velocity perpendicular to the magnetic field was small (less than 50 km/s), implying that the BBF does not contribute to the finger-like structures. The development speeds of the finger-like structures estimated from auroral images are comparable to the observed perpendicular ion velocity.

In a near-conjugate event, observed at Gakona (MLAT: 63.1°N), Alaska, the whole auroral structure expanded southward, while finger-like structures started to develop northward at 1300 UT. The footprint of THEMIS-D moved northwestward during the development of the finger-like structures over Fort Yukon, north of Gakona. The variation of the plasma and magnetic pressures again showed antiphase fluctuations. The ion velocities perpendicular to the magnetic field are also small (less than 100 km/s) compared to the BBF.

In this paper we investigated the plasma and magnetic field variations at the equatorial plane of the magnetosphere near the conjugate location of the auroral finger-like structures. However, we found that only one conjugate event and only one satellite observed the variations of the magnetospheric magnetic field connected to the source region of the finger-like structures in the event. Because of the small number of conjugate events, we have not obtained sufficient data to elucidate the physical process causing the auroral finger-like structures. Additional observations using other magnetospheric satellites (e.g., RBSP and ERG) will be needed to understand the mechanism for the generation of finger-like structures. There is also still room to examine phase relationships between plasma and magnetic pressures in the magnetosphere, because antiphase pressure fluctuation is seen in both cases.

Acknowledgments
The Conjunction Event Finder at DARTS JAXA/ISAS provided useful information for this study. We acknowledge NASA contract NAS5-02099 and V. Angelopoulos for the use of data from the THEMIS mission. Specifically, we thank C.W. Carlson and J.P. Mcfadden for use of ESA data; J.W. Bonnell and F.S. Mozer for use of EFI data; D. Larson for use of SST data; K.H. Glassmeier, U. Auster, and W. Baumjohann for the use of FGM data provided under the lead of the Technical University of Braunschweig and with financial support through the German Ministry for Economy and Technology and the German Center for Aviation and Space (DLR) under contract 50 OC 0302; S. Mende and E. Donovan for use the ASI data, the CSA for logistical support in fielding and data retrieval from the GBO stations, and NSF for support of GIMNAST through grant AGS-1004736; S. Mende and C.T. Russell for use of the GMAG data and NSF for support through grant AGS-1004814; and I.R. Mann, D.K. Milling, and the rest of the CARISMA team for use of GMAG data. CARISMA is operated by the University of Alberta, funded by the Canadian Space Agency. Data provided by the Geophysical Institute Magnetometer Array operated by the Geophysical Institute, University of Alaska. More information about this data set is available at http://magnet.asf.alaska.edu/, and magnetometer data from the Greenland Magnetometer Array were provided by the National Space Institute at the Technical University of Denmark. THEMIS probes, geomagnetic field, and all-sky image data are available through the open data repository at UC Berkeley at http://themis.ssl.berkeley.edu/index.shtml. The T96 model was obtained from the GSFC/SPDF OMNIWeb interface at http://omniweb.gsfc.nasa.gov. This work was supported by KAKENHI grants 15H05815 and 16H06286 provided by the Japan Society for the Promotion of Science.

References

Angelopoulos, V. (2008), The THEMIS misson, *Space Sci. Rev.*, *141*, 5–34, doi:10.1007/s11214-008-9336-1.
Angelopoulos, V., W. Baumjohann, C. F. Kennek, F. V. Corontti, M. G. Kivelson, R. Pellat, R. J. Walker, H. Lohr, and G. Paschmann (1992), Bursty bulk flows in the inner central plasma sheet, *J. Geophys. Res.*, *97*(A4), 4027–4039.
Angelopoulos, V., et al. (2008), First results from the THEMIS mission, *Space. Sci. Rev.*, *141*, 453–476, doi:10.1007/s11214-008-9378-4.
Auster, H. U., et al. (2008), The THEMIS fluxgate magnetometer, *Space Sci. Rev.*, *141*, 235–264, doi:10.1007/s11214-008-9365-9.
Bonnell, J. W., F. S. Mozer, G. T. Delory, A. J. Hull, R. E. Ergun, C. M. Cully, V. Angelopoulos, and P. R. Harvey (2008), The Electric Field Instrument (EFI) for THEMIS, *Space Sci. Rev.*, *141*, 303–341, doi:10.1007/s11214-008-9469-2.
Cheng, C. Z. (2004), Physics of substorm growth phase, onset, and dipolarization, *Space Sci. Rev.*, *113*, 207–270.
Davis, T. N. (1978), Observed characteristics of auroral forms, *Space Sci. Rev.*, *22*(1), 77–113.
Donovan, E., et al. (2008), Simultaneous THEMIS in situ and auroral observations of a small substorm, *Geophys. Res. Lett.*, *35*, L17S18, doi:10.1029/2008GL033794.
Ebihara, Y., T. Sakanoi, K. Asamura, M. Hirahara, and M. F. Thomsen (2010), Reimei observation of highly structured auroras caused by nonaccelerated electrons, *J. Geophys. Res.*, *115*, A08320, doi:10.1029/2009JA015009.
Ejiri. M., R. A. Hoffman, and P. H. Smith (1980), Energetic particle penetrations into the inner magnetosphere, *J. Geophys. Res.*, *85*(A2), 653–663.
Gold, T. (1959), Motions in the magnetosphere of the Earth, *J. Geophys. Res.*, *64*(9), 1219–1224.
Haerendel, G. (2007), Auroral arcs as sites of magnetic stress release, *J. Geophys. Res.*, *112*, A09214, doi:10.1029/2007JA012378.
Harris, S. E., et al. (2008), THEMIS ground based observatory system design, *Space Sci. Rev.*, *141*, 213–233, doi:10.1007/s11214-007-9294-z.
Hasegawa, A., and T. Sato (1979), Generation of field aligned current during substorm, in *Dynamics of the Magnetosphere*, edited by S.-I. Akasofu, pp. 529–542, D. Reidel, Norwell, Mass.
Hashimoto, A., K. Shiokawa, Y. Otsuka, S.-I. Oyama, S. Nozawa, T. Hori, M. Lester, and M. G. Johnsen (2015), Statistical study of auroral fragmentation into patches, *J. Geophys. Res. Space Physics*, *120*, 6207–6217, doi:10.1002/2015JA021000.
Kennel, C. F., and H. E. Petschek (1966), Limit on stably trapped particle fluxes, *J. Geophys. Res.*, *71*, 1.
Kistler, L. M., E. Möbius, W. Baumjohann, and G. Paschmann (1992), Pressure changes in the plasma sheet during substorm injections, *J. Geophys. Res.*, *A3*, 2973–2983.
Kozlovsky, A., A. Aikio, T. Turunen, H. Nilsson, T. Sergienko, V. Safargaleev, and K. Kauristie (2007), Dynamics and electric currents of morningside Sun-aligned auroral arcs, *J. Geophys. Res.*, *112*, A06306, doi:10.1029/2006JA012244.
Larson, D. (2009), Using the THEMIS energetic particle data. [Available at http://www.virbo.org/Image:THEMIS-SST.pp.]
Liang, J., V. Uritsky, E. Donovan, B. Ni, E. Spanswick, T. Trondsen, J. Bonnell, A. Roux, U. Auster, and D. Larson (2010), THEMIS observations of electron cyclotron harmonic emissions, ULF waves, and pulsating auroras, *J. Geophys. Res.*, *115*, A10235, doi:10.1029/2009JA015148.
McFadden, J. P., C. W. Carlson, D. Larson, M. Ludlam, R. Ablad, B. Elliott, P. Turin, M. Marckwordt, and V. Angelopoulos (2008), The THEMIS ESA plasma instrument and in-flight calibration, *Space Sci. Rev.*, *141*, 277–302, doi:10.1007/s11214-008-9440-2.
Mende, S. B., S. E. Harris, H. U. Frey, V. Angelopoulos, C. T. Russell, E. Donovan, B. Jackel, M. Greffen, and L. M. Peticolas (2008), The THEMIS array of ground-based observatories for the study of auroral substorms, *Space Sci. Rev.*, *141*, 357–387, doi:10.1007/s11214-008-9380-x.
Mendillo, M., J. Baumgardner, and J. Providakes (1989), Ground-based imaging of detached arcs, ripples in the diffuse aurora, and patches of 6300-Å emission, *J. Geophys. Res*, *94*(A5), 5367–5381.

Miura, A. (2009), Pressure-driven and ionosphere-driven modes of magnetospheric interchange instability, *J. Geophys. Res*, *114*, A02224, doi:10.1029/2008JA013663.

Miyashita, Y., I. Shinohara, M. Fujimoto, H. Hasegawa, K. Hosokawa, T. Takada, and T. Hori (2011), A powerful tool for quick-look data in solar-terrestrial physics "Conjunction Event Finder", *Earth Planets Space*, *63*, e1–e4.

Nakajima, A., et al. (2012), Electron and wave characteristics observed by the THEMIS satellites near the magnetic equator during a pulsating aurora, *J. Geophys. Res.*, *117*, A03219, doi:10.1029/2011JA017066.

Nakamura, R., and T. Oguti (1987), Drifts of auroral structures and magnetospheric electric fields, *J. Geophys. Res.*, *92*, 11,241–11,247.

Nishitani, N., G. Hough, and M. W. J. Scourfield (1994), Spatial and temporal characteristics of giant undulations, *J. Geophys. Res.*, *21*, 2673–2676.

Rae, I. J., I. R. Mann, C. E. J. Watt, L. M. Kistler, and W. Baumjohann (2007), Equator-S observations of drift mirror mode waves in the dwanside magnetosphere, *J. Geophys. Res.*, *112*, A11203, doi:10.1029/2006JA012064.

Reiff, P. H., H. L. Collin, J. D. Craven, J. L. Burch, J. D. Winningham, E. G. Shelly, L. A. Frank, and M. A. Friedman (1988), Determination of auroral electron potentials using high- and low-altitude particle distributions, *J. Geophys. Res.*, *93*, 7441–7465.

Sato, N., A. Kadokura, Y. Tanaka, T. Nishiyama, T. Hori, and A. S. Yukimatu (2015), Omega band pulsating auroras observed onboard THEMIS spacecraft and on the ground, *J. Geophys. Res. Space Physics*, *120*, 5524–5544, doi:10.1002/2015JA021382.

Shiokawa, K., A. Nakajima, A. Ieda, K. Sakaguchi, R. Nomura, T. Aslaksen, M. Greffen, and E. Donovan (2010), Rayleigh-Taylor type instability in auroral patches, *J. Geophys. Res.*, *115*, A02211, doi:10.1029/2009JA014273.

Shiokawa, K., et al. (2014), Auroral fragmentation into patches, *J. Geophys. Res. Space Physics*, *119*, 8249–8261, doi:10.1002/2014JA020050.

Treumann, R. A., and W. Baumjohann (1997), *Advanced Space Plasma Physics*, 381 pp., Imperial College Press, London.

Tsyganenko, N. A., and D. P. Stern (1996), Modeling the global magnetic field of the large-scale Birkeland current systems, *J. Geophys. Res.*, *101*(A12), 27,187–27,198.

Vaivads, A., W. Baumjohann, G. Haerendel, R. Nakamura, H. Kucharek, B. Klecker, M. R. Lessard, L. M. Kistler, T. Mukai, and A. Nishida (2001), Compressional Pc5 type pulsations in the morningside plasma sheet, *Ann. Geophys.*, *19*, 311–320.

Voronkov, I., R. Rankin, P. Frycz, V. T. Tikhonchuk, and J. C. Samson (1997), Coupling of shear flow and pressure gradient instabilities, *J. Geophys. Res.*, *102*, 9639–9650.

Xing, X., and R. A. Wolf (2007), Criterion for interchange instability in a plasma connected to a conducting ionosphere, *J. Geophys. Res.*, *112*, A12209, doi:10.1029/2007JA012535.

Zhang, Y., C.-I. Meng, L. J. Paxton, D. Morrison, B. Wolven, H. Kil, P. Newell, S. Wing, and A. B. Christensen (2005), Far-ultraviolet signature of polar cusp during southward IMF B_z observed by TIMED/Global Ultraviolet Imager and DMSP, *J. Geophys. Res.*, *110*, A01218, doi:10.1029/2004JA010707.